

Topological Diagrams and Hadronic Weak Decays of Charmed Baryons

Huiling Zhong and Fanrong Xu*

*Department of Physics, College of Physics & Optoelectronic Engineering,
Jinan University, Guangzhou 510632, P.R. China*

Hai-Yang Cheng

Institute of Physics, Academia Sinica, Taipei, Taiwan 11529, Republic of China

(Dated: January 30, 2024)

Inspired by the recent BESIII measurement of the decay asymmetry and the phase shift between S - and P -wave amplitudes in the decay $\Lambda_c^+ \rightarrow \Xi^0 K^+$, we perform a global fit to the experimental data of charmed baryon decays based on the topological diagrammatic approach (TDA) which has the advantage that it is more intuitive and easier to implement model calculations. The measured branching fractions and decay asymmetries are well accommodated in TDA except for two modes, in particular, the predicted $\mathcal{B}(\Xi_c^0 \rightarrow \Xi^- \pi^+) = (2.64 \pm 0.13)\%$ is larger than its current value. The predicted magnitudes of S - and P -wave amplitudes and their phase shifts are presented for measured and yet-to-be-measured modes which can be tested in forthcoming experiments.

1. Introduction— Both experimental and theoretical progresses in the study of hadronic decays of charmed baryons were very slow for a long time. The situation was reversed since 2014 as there were several major breakthroughs in charmed-baryon experiments in regard to the weak decays of Λ_c^+ and $\Xi_c^{+,0}$ (for a review, see Ref. [1]). Consider the decay $\mathcal{B}_i \rightarrow \mathcal{B}_f + P$ with P being a pseudoscalar meson and \mathcal{B}_i , \mathcal{B}_f the initial- and final-state baryon, respectively, its general decay amplitude reads

$$M(\mathcal{B}_i \rightarrow \mathcal{B}_f + P) = i\bar{u}_f(A - B\gamma_5)u_i, \quad (1)$$

where A and B correspond to the parity-violating S -wave and parity-conserving P -wave amplitudes, respectively. They generally receive both factorizable and nonfactorizable contributions. In the 1990s various approaches such as the relativistic quark model, the pole model and current algebra were developed to describe the nonfactorizable effects in hadronic decays of charmed baryons [1].

Besides the dynamical model calculations, nonleptonic decays of charmed baryons also have been analyzed using the symmetry approaches such as the irreducible $SU(3)$ approach (IRA) and the topological diagrammatic approach (TDA). These approaches, especially IRA, have become very popular in the past few years. After the pioneer work in Ref. [2], it became a common practice to perform a global fit of both S - and P -wave parameters to the data of branching fractions and decay asymmetries. Just like the case of hyperon decays, non-trivial relative strong phases between S - and P -wave amplitudes may exist, but they are usually neglected in the model calculations.

There is one decay mode that deserves special attention, namely, the Cabibbo-favored decay $\Lambda_c^+ \rightarrow \Xi^0 K^+$ which proceeds only through W -exchange. Early studies in 1990's indicated that its S - and P -wave amplitudes

are very small due to strong cancellation between various terms (see e.g. Ref. [3]). For example, the use of current algebra implies a vanishing S -wave in the $SU(3)$ limit. Consequently, the calculated branching fraction is too small compared to experiment and the predicted α is zero owing to the vanishing S -wave amplitude. It is thus striking that the approach based on IRA tends to predict a large decay asymmetry close to unity [2, 4, 5]. It is also true in a revised pole model calculation in Ref. [6]. This long-standing puzzle was recently resolved by a new BESIII measurement [7]. Not only the decay asymmetry $\alpha_{\Xi^0 K^+} = 0.01 \pm 0.16$ was found to be consistent with zero, but also the measured Lee-Yang parameter $\beta_{\Xi^0 K^+} = -0.64 \pm 0.69$ was nonzero, implying a phase difference between S - and P -wave amplitudes, $\delta_P - \delta_S = -1.55 \pm 0.25$ or 1.59 ± 0.25 rad. Since $|\cos(\delta_P - \delta_S)| \sim 0.02$, this accounts for the smallness of $\alpha_{\Xi^0 K^+}$.

Recently, a new analysis of charmed baryon decays based on IRA that takes into account the phase shifts of the partial-wave amplitudes has been put forward in Ref. [8]. In this work we shall perform a similar study within the framework of TDA. Since TDA has been applied very successfully to charmed meson decays [9–11], it is conceivable that the same approach is applicable to the charmed baryon sector. TDA has the advantage that it is more intuitive and easier to implement model calculations. For the recent analysis of hadronic charmed baryon decays in TDA, see Refs. [12, 13].

2. Formalism— Since baryons are made of three quarks in contrast to two quarks for the mesons, the application of TDA to the baryon case will inevitably lead to some complications. For example, the symmetry of the quarks in flavor space could be different. The first analysis of two-body nonleptonic decays of antitriplet charmed baryons in TDA was carried out by Kohara [14]. A subsequent study was given by Chau, Cheng and Tseng (CCT) in Ref. [15]. The difference between Kohara and CCT

* fanrongxu@jnu.edu.cn

lies in the choice of the wave functions of octet baryons:

$$|\mathcal{B}^{m,k}(8)\rangle = a|\chi^m(1/2)_{A_{12}}\rangle|\psi^k(8)_{A_{12}}\rangle + b|\chi^m(1/2)_{S_{12}}\rangle|\psi^k(8)_{S_{12}}\rangle \quad (2)$$

with $|a|^2 + |b|^2 = 1$ in Ref. [15], and

$$|\tilde{\mathcal{B}}^{m,k}(8)\rangle = \alpha|\chi^m(1/2)_{A_{12}}\rangle|\psi^k(8)_{A_{12}}\rangle + \beta|\chi^m(1/2)_{A_{23}}\rangle|\psi^k(8)_{A_{23}}\rangle \quad (3)$$

in Ref. [14], where $\chi^m(1/2)_{A,S}$ are the spin parts of the wave function defined in Eq. (23) of Ref. [15] and

$$\begin{aligned} |\psi^k(8)_{A_{12}}\rangle &= \sum_{q_a, q_b, q_c} |[q_a q_b] q_c] \langle [q_a q_b] q_c | \psi^k(8)_{A_{12}} \rangle, \\ |\psi^k(8)_{S_{12}}\rangle &= \sum_{q_a, q_b, q_c} |\{q_a q_b\} q_c\rangle \langle \{q_a q_b\} q_c | \psi^k(8)_{S_{12}} \rangle \end{aligned} \quad (4)$$

denote the octet baryon states that are antisymmetric and symmetric in the first two quarks, respectively. As shown explicitly in Ref. [16], physics is independent of the convention one chooses. The TDA amplitudes expressed in the schemes with $\mathcal{B}^{m,k}(8)$ and $\tilde{\mathcal{B}}^{m,k}(8)$ are equivalent. Nevertheless, we prefer to use the bases $\psi^k(8)_{A_{12}}$ and $\psi^k(8)_{S_{12}}$ as they are orthogonal to each other, while $\psi^k(8)_{A_{12}}$ and $\psi^k(8)_{A_{23}}$ are not.

In terms of the octet baryon wave functions given in Eq. (2), the relevant topological diagrams for the decay $\mathcal{B}_c(\bar{3}) \rightarrow \mathcal{B}(8)M(8+1)$ are depicted in Fig. 1: the external W -emission, T ; the internal W -emission C ; the inner W -emission C' ; W -exchange diagrams E_{1A} , E_{1S} , E_{2A} , E_{2S} , E_3 and the hairpin diagram E_h . The decay amplitudes of $\mathcal{B}_c(\bar{3}) \rightarrow \mathcal{B}(8)M(8+1)$ in TDA have the expressions:

$$\begin{aligned} \mathcal{A}_{\text{TDA}} = & T(\mathcal{B}_c)^{ij} H_l^{km} (\mathcal{B}_8)_{ijk} M_m^l \\ & + C(\mathcal{B}_c)^{ij} H_k^{ml} (\mathcal{B}_8)_{ijl} M_m^k \\ & + C'(\mathcal{B}_c)^{ij} H_m^{kl} (\mathcal{B}_8)_{klj} M_i^m \\ & + E_{1A}(\mathcal{B}_c)^{ij} H_i^{kl} (\mathcal{B}_8)_{jkm} M_l^m \\ & + E_{1S}(\mathcal{B}_c)^{ij} H_i^{kl} M_l^m \left[(\mathcal{B}_8)_{jmk} + (\mathcal{B}_8)_{kmj} \right] \quad (5) \\ & + E_{2A}(\mathcal{B}_c)^{ij} H_i^{kl} (\mathcal{B}_8)_{jlm} M_k^m \\ & + E_{2S}(\mathcal{B}_c)^{ij} H_i^{kl} M_k^m \left[(\mathcal{B}_8)_{jml} + (\mathcal{B}_8)_{lmj} \right] \\ & + E_3(\mathcal{B}_c)^{ij} H_i^{kl} (\mathcal{B}_8)_{klm} M_j^m \\ & + E_h(\mathcal{B}_c)^{ij} H_i^{kl} (\mathcal{B}_8)_{klj} M_m^m, \end{aligned}$$

where $(\mathcal{B}_c)^{ij}$ is an antisymmetric baryon matrix standing for antitriplet charmed baryons, $(\mathcal{B}_8)_j^i$ and M_j^i represent octet baryons and nonet mesons, respectively, see e.g. Refs. [12, 18] for their explicit expressions. Based on the convention of $(\mathcal{B}_8)_j^i$, we adopt the notation $(\mathcal{B}_8)_{ijk} = \epsilon_{ijl}(\mathcal{B}_8)_k^l$ to describe the baryon octet. The H matrix is related to the CKM mixing matrix with the non-vanishing elements: $H_2^{31} = V_{cs}^* V_{ud}$, $H_3^{31} = V_{cs}^* V_{us}$, $H_2^{21} = V_{cd}^* V_{ud}$ and $H_3^{21} = V_{cd}^* V_{us}$.

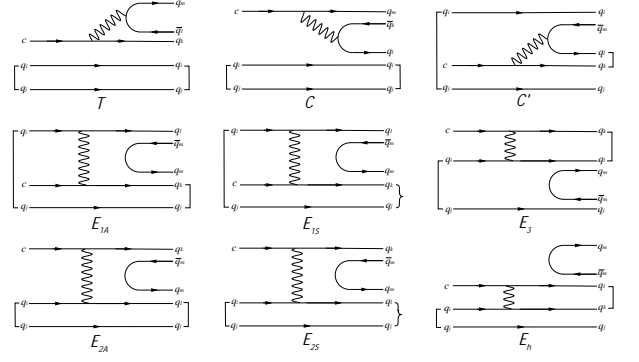


FIG. 1. Topological diagrams contributing to $\mathcal{B}_c(\bar{3}) \rightarrow \mathcal{B}(8)M(8+1)$ decays.

Note that there are 7 topological diagrams in Ref. [12] corresponding to 19 TDA amplitudes. However, in diagrams T and C , the two spectator quarks q_i and q_j are antisymmetric in flavor. Moreover, the final-state quarks q_l and q_k in topological diagrams C' , E_3 and E_h must be antisymmetric in flavor owing to the Körner-Pati-Woo theorem which states that the quark pair in a baryon produced by weak interactions is required to be antisymmetric in flavor [17]. Consequently, the number of TDA amplitudes is reduced from 19 to 11. Next, one needs to consider the symmetric and antisymmetric parts of $E_{1,2}$ diagrams separately. As a result, the number of TDA amplitudes is further reduced from 11 to 9. Therefore, the number of topological diagrams and TDA amplitudes is 9 as shown in Fig. 1 and Eq. (5).

Working out Eq. (5) for $\mathcal{B}_c(\bar{3}) \rightarrow \mathcal{B}(8)M(8+1)$ decays, we obtain the TDA decay amplitudes listed in Table I. For complete TDA amplitudes of singly- and doubly-Cabibbo-suppressed decays, see Ref. [18]. The expressions of TDA amplitudes agree with CCT [15] through the following relations:

$$\begin{aligned} \mathcal{A}_A &= -4T, \quad \mathcal{B}_A = 2C', \quad \mathcal{B}'_A = -4C, \\ \mathcal{C}_{1A} &= 2E_3, \quad \mathcal{C}_{2A} = 2E_{1A}, \quad \mathcal{C}'_A = 2E_{2A}, \quad (6) \\ \mathcal{C}_{2S} &= -2\sqrt{3}E_{1S}, \quad \mathcal{C}'_S = -2\sqrt{3}E_{2S}, \end{aligned}$$

where \mathcal{A}_A , \mathcal{B}_A , \mathcal{B}'_A , \mathcal{C}_{1A} , \mathcal{C}_{2A} , \mathcal{C}'_A , \mathcal{C}_{2S} and \mathcal{C}'_S are the TDA amplitudes defined in Ref. [15]. The agreement is non-trivial in view of the different approaches adopted in Ref. [15] and here. Among the 9 TDA amplitudes given in Eq. (5), there still exist 2 redundant degrees of freedom through the redefinition [15]:

$$\begin{aligned} \tilde{T} &= T - E_{1S}, \quad \tilde{C} = C - E_{2S}, \\ \tilde{C}' &= C' + 2E_{2S}, \quad \tilde{E}_1 = E_{1A} + E_{1S} - E_3, \quad (7) \\ \tilde{E}_2 &= E_{2A} + E_{2S} + E_3, \quad \tilde{E}_3 = E_{1S} + E_{2S}, \\ \tilde{E}_h &= E_h + \frac{2}{3}E_{1S} - \frac{4}{3}E_{2S}. \end{aligned}$$

Many relations can be easily derived from Table I, which will be discussed in detail in Ref. [18]. One of

TABLE I. TDA amplitudes for CF (upper part) and several SCS (lower part) $\mathcal{B}_c(3) \rightarrow \mathcal{B}(8)M(8+1)$ decays. The amplitudes for CF (SCS) decays have to be multiplied by the matrix element H_2^{31} (H_3^{31} or H_2^{21} , depending on the process). For the η and η' mesons, we take $\eta = \cos\theta\eta_8 - \sin\theta\eta_1$, $\eta' = \sin\theta\eta_8 + \cos\theta\eta_1$ with $\theta \approx -15^\circ$.

Channel	TDA
$\Lambda_c^+ \rightarrow \Lambda\pi^+$	$\frac{1}{\sqrt{6}}(-4T + C' + E_{1A} + 3E_{1S} - E_3)$
$\Lambda_c^+ \rightarrow \Sigma^0\pi^+$	$\frac{1}{\sqrt{2}}(-C' - E_{1A} + E_{1S} + E_3)$
$\Lambda_c^+ \rightarrow \Sigma^+\pi^0$	$\frac{1}{\sqrt{2}}(C' + E_{1A} - E_{1S} - E_3)$
$\Lambda_c^+ \rightarrow \Sigma^+\eta_8$	$\frac{1}{\sqrt{6}}(-C' + E_{1A} - E_{1S} - 4E_{2S} - E_3)$
$\Lambda_c^+ \rightarrow \Sigma^+\eta_1$	$\frac{1}{\sqrt{3}}(-C' + E_{1A} - E_{1S} + 2E_{2S} - E_3 - 3E_h)$
$\Lambda_c^+ \rightarrow \Xi^0 K^+$	$E_{1A} + E_{1S} - E_3$
$\Lambda_c^+ \rightarrow p\bar{K}^0$	$2C - 2E_{2S}$
$\Xi_c^0 \rightarrow \Lambda\bar{K}^0$	$\frac{1}{\sqrt{6}}(2C - C' + E_{2A} - 3E_{2S} + E_3)$
$\Xi_c^0 \rightarrow \Sigma^0\bar{K}^0$	$\frac{1}{\sqrt{2}}(2C + C' - E_{2A} - E_{2S} - E_3)$
$\Xi_c^0 \rightarrow \Sigma^+ K^-$	$E_{2A} + E_{2S} + E_3$
$\Xi_c^0 \rightarrow \Xi^0\pi^0$	$\frac{1}{\sqrt{2}}(-C' + 2E_{1S})$
$\Xi_c^0 \rightarrow \Xi^0\eta_8$	$\frac{1}{\sqrt{6}}(C' + 2E_{1S} - 2E_{2A} + 2E_{2S} - 2E_3)$
$\Xi_c^0 \rightarrow \Xi^0\eta_1$	$\frac{1}{\sqrt{3}}(C' + 2E_{1S} + E_{2A} - E_{2S} + E_3 + 3E_h)$
$\Xi_c^0 \rightarrow \Xi^-\pi^+$	$2T - 2E_{1S}$
$\Xi_c^+ \rightarrow \Sigma^+\bar{K}^0$	$-2C - C'$
$\Xi_c^+ \rightarrow \Xi^0\pi^+$	$-2T + C'$
$\Lambda_c^+ \rightarrow \Lambda K^+$	$\frac{1}{\sqrt{6}}(-4T + C' - 2E_{1A} + 2E_3)$
$\Lambda_c^+ \rightarrow \Sigma^0 K^+$	$\frac{1}{\sqrt{2}}(-C' + 2E_{1S})$
$\Lambda_c^+ \rightarrow \Sigma^+ K^0$	$-C' - 2E_{2S}$
$\Lambda_c^+ \rightarrow p\pi^0$	$\frac{1}{\sqrt{2}}(2C + C' + E_{1A} - E_{1S} - 2E_{2S} - E_3)$
$\Lambda_c^+ \rightarrow p\eta_8$	$\frac{1}{\sqrt{6}}(-6C + C' + E_{1A} - E_{1S} + 2E_{2S} - E_3)$
$\Lambda_c^+ \rightarrow p\eta_1$	$\frac{1}{\sqrt{3}}(-C' + E_{1A} - E_{1S} + 2E_{2S} - E_3 - 3E_h)$
$\Lambda_c^+ \rightarrow n\pi^+$	$-2T + C' + E_{1A} + E_{1S} - E_3$
$\Xi_c^0 \rightarrow \Xi^- K^+$	$2T - 2E_{1S}$

them is

$$\frac{\tau_{\Lambda_c^+}}{\tau_{\Xi_c^0}} \mathcal{B}(\Xi_c^0 \rightarrow \Xi^-\pi^+) = \mathcal{B}(\Lambda_c^+ \rightarrow \Sigma^0\pi^+) + 3\mathcal{B}(\Lambda_c^+ \rightarrow \Lambda\pi^+) - \frac{1}{\sin^2\theta_C} \mathcal{B}(\Lambda_c^+ \rightarrow n\pi^+). \quad (8)$$

This relation first derived in Ref. [8] is very useful in constraining the branching fraction of $\Xi_c^0 \rightarrow \Xi^-\pi^+$.

3. Numerical Analysis and Results— As there are 7 independent tilde TDA amplitudes given in Eq. (7), we have totally 28 unknown parameters to describe the magnitudes and the phases of the respective S - and P -wave amplitudes, namely, $|\tilde{T}|_S e^{i\delta_S^{\tilde{T}}}$, $|\tilde{C}|_S e^{i\delta_S^{\tilde{C}}}$, \dots , $|\tilde{E}_h|_S e^{i\delta_S^{\tilde{E}_h}}$, $|\tilde{T}|_P e^{i\delta_P^{\tilde{T}}}$, \dots , $|\tilde{E}_h|_P e^{i\delta_P^{\tilde{E}_h}}$, collectively denoted by $|X_i|_S e^{i\delta_S^{X_i}}$ and $|X_i|_P e^{i\delta_P^{X_i}}$, where the subscripts S and P denote the S - and P -wave components of each TDA amplitude. Since there is an overall phase which can be omitted, we shall set $\delta_S^{\tilde{T}} = 0$. Hence, we are left with 27 parameters. Notice that the number of available experimental observables has increased to 30 by the end of 2023. To pursue a set of proper parameters, the χ^2 function in the following maximum likelihood analysis is

TABLE II. Fitted tilde TDA amplitudes collectively denoted by X_i .

	$ X_i _S$ ($10^{-2}G_F$)	$ X_i _P$	$\delta_S^{X_i}$ (in radian)	$\delta_P^{X_i}$
\tilde{T}	2.15 ± 0.17	16.22 ± 0.44	—	2.79 ± 0.11
\tilde{C}	1.78 ± 1.74	13.49 ± 1.53	0.48 ± 0.62	-0.78 ± 0.32
\tilde{C}'	3.32 ± 0.65	27.26 ± 2.56	-1.51 ± 0.29	2.14 ± 0.15
\tilde{E}_1	4.69 ± 0.31	1.48 ± 1.30	-1.90 ± 0.14	2.29 ± 0.90
\tilde{E}_2	0.72 ± 8.33	11.83 ± 4.72	-1.98 ± 2.52	1.10 ± 0.57
\tilde{E}_3	1.97 ± 0.40	5.39 ± 1.80	-1.96 ± 0.21	0.92 ± 0.27
\tilde{E}_h	1.83 ± 1.27	19.88 ± 5.45	-0.09 ± 0.50	-1.53 ± 0.26

defined as

$$\chi^2 = [\mathcal{O}_{\text{theor}}(c_i) - \mathcal{O}_{\text{expt}}]^T \Sigma^{-1} [\mathcal{O}_{\text{theor}}(c_i) - \mathcal{O}_{\text{expt}}], \quad (9)$$

in which c_i are the fitted 27 input parameters, $\mathcal{O}_{\text{theor}, \text{expt}}$ stand for the 30 theoretical and experimental observables. The 30-dimensional general error matrix Σ can be taken diagonal by neglecting correlations among different observables and only incorporating pure experimental errors here. In addition to the latest PDG values [19] adopted as partial inputs in χ^2 , more Λ_c^+ related data have been supplied by BESIII in 2023, including branching fractions of $\Lambda_c^+ \rightarrow p\pi^0$ [20] and $\Lambda_c^+ \rightarrow p\eta$ [7]. Likewise, Belle has also contributed the recent measurements to Ξ_c^0 , such as $\Xi_c^0 \rightarrow \Xi^-\pi^+$ [21] and $\Xi_c^0 \rightarrow \Lambda^0 K_S, \Sigma^0 K_S, \Sigma^+ K^-$ [22].

In terms of the S - and P -wave amplitudes given in Eq. (1) and their phases δ_S and δ_P , respectively, the decay rate and decay asymmetries read

$$\begin{aligned} \Gamma &= \frac{p_c}{8\pi} \frac{(m_i + m_f)^2 - m_P^2}{m_i^2} (|A|^2 + \kappa^2 |B|^2), \\ \alpha &= \frac{2\kappa |A||B| \cos(\delta_P - \delta_S)}{|A|^2 + \kappa^2 |B|^2}, \quad \beta = \frac{2\kappa |A||B| \sin(\delta_P - \delta_S)}{|A|^2 + \kappa^2 |B|^2}, \\ \gamma &= \frac{|A|^2 - \kappa^2 |B|^2}{|A|^2 + \kappa^2 |B|^2}, \end{aligned} \quad (10)$$

where p_c is the c.m. three-momentum in the rest frame of the initial baryon and the auxiliary parameter κ is defined as $\kappa = p_c/(E_f + m_f)$. The available experimental data are collected in Table III below. Note that for Ξ_c^0 decays, many of the modes are measured relative to $\Xi_c^0 \rightarrow \Xi^-\pi^+$; that is, $\mathcal{R}_X \equiv \mathcal{B}(\Xi_c^0 \rightarrow X)/\mathcal{B}(\Xi_c^0 \rightarrow \Xi^-\pi^+)$ for $X = \Xi^- K^+, \Lambda^0 K_S^0, \Sigma^0 K_S^0$ and $\Sigma^+ K^-$.

In practice, we shall make use of the package `iminuit` [23, 24] to search for χ_{min}^2 together with its corresponding fitted parameters c_i exhibited in Table II, and generate the covariance matrix among parameters which further helps predict physical observables. The fit branching fractions, decay asymmetries, the magnitudes of S and P waves and their phase shifts are shown in Tables III and IV. Owing to the space limit, the fitted parameters β and γ will be presented in Ref. [18]. We see

TABLE III. The fit results based on the tilde TDA. S - and P -wave amplitudes are in units of $10^{-2}G_F$ and $\delta_P - \delta_S$ in radian.

Channel	$10^2\mathcal{B}$	α	$ A $	$ B $	$\delta_P - \delta_S$	$10^2\mathcal{B}_{\text{exp}}$	α_{exp}
$\Lambda_c^+ \rightarrow \Lambda^0 \pi^+$	1.28 ± 0.05	-0.76 ± 0.01	3.63 ± 0.27	15.26 ± 0.63	-0.63 ± 0.06	1.29 ± 0.05	-0.76 ± 0.01 [19, 26]
$\Lambda_c^+ \rightarrow \Sigma^0 \pi^+$	1.26 ± 0.05	-0.48 ± 0.02	2.77 ± 0.38	18.20 ± 0.64	0.92 ± 2.53	1.27 ± 0.06	-0.47 ± 0.03 [19, 26]
$\Lambda_c^+ \rightarrow \Sigma^+ \pi^0$	1.27 ± 0.05	-0.48 ± 0.02	2.77 ± 0.38	18.20 ± 0.64	0.92 ± 2.53	1.25 ± 0.09	-0.49 ± 0.03 [19, 25]
$\Lambda_c^+ \rightarrow \Sigma^+ \eta$	0.32 ± 0.04	-0.99 ± 0.05	2.28 ± 0.51	9.43 ± 1.60	-0.04 ± 0.50	0.32 ± 0.04 [19, 25]	-0.99 ± 0.06 [25]
$\Lambda_c^+ \rightarrow \Sigma^+ \eta'$	0.44 ± 0.14	-0.46 ± 0.07	4.03 ± 1.88	24.64 ± 6.52	1.09 ± 0.84	0.44 ± 0.15 [19, 25]	-0.46 ± 0.07 [25]
$\Lambda_c^+ \rightarrow \Xi^0 K^+$	0.53 ± 0.07	-0.07 ± 0.14	4.46 ± 0.29	1.40 ± 1.24	-2.10 ± 0.91	0.55 ± 0.07	0.01 ± 0.16 [7]
$\Lambda_c^+ \rightarrow \Lambda^0 K^+$	0.0635 ± 0.003	-0.57 ± 0.05	0.90 ± 0.10	3.83 ± 0.26	0.93 ± 0.07	0.0635 ± 0.0031 [19, 26]	-0.585 ± 0.052 [26]
$\Lambda_c^+ \rightarrow \Sigma^0 K^+$	0.0370 ± 0.0039	-0.32 ± 0.13	0.27 ± 0.09	3.97 ± 0.21	-0.79 ± 0.34	0.0382 ± 0.0051 [19, 26]	-0.55 ± 0.20 [26]
$\Lambda_c^+ \rightarrow \Sigma^+ K_S$	0.047 ± 0.008	-0.63 ± 0.11	0.73 ± 0.14	5.97 ± 0.56	0.51 ± 4.28	0.047 ± 0.014	
$\Lambda_c^+ \rightarrow n \pi^+$	0.073 ± 0.010	-0.88 ± 0.09	1.27 ± 0.11	2.05 ± 0.32	-0.30 ± 0.19	0.066 ± 0.013	
$\Lambda_c^+ \rightarrow p \pi^0$	0.02 ± 0.01	-0.06 ± 1.21	0.64 ± 0.23	0.71 ± 1.23	1.49 ± 1.59	$0.0156^{+0.0075}_{-0.0061}$ [20]	
$\Lambda_c^+ \rightarrow p K_S$	1.59 ± 0.07	0.18 ± 0.40	3.38 ± 3.33	25.64 ± 2.91	-1.26 ± 0.78	1.59 ± 0.07	0.18 ± 0.45
$\Lambda_c^+ \rightarrow p \eta$	0.149 ± 0.008	0.49 ± 0.49	1.09 ± 0.80	5.32 ± 1.10	-0.94 ± 0.85	0.149 ± 0.008 [19, 20, 27]	
$\Lambda_c^+ \rightarrow p \eta'$	0.049 ± 0.009	-0.42 ± 0.49	0.65 ± 0.47	4.74 ± 0.91	0.98 ± 0.47	0.049 ± 0.009	
$\Xi_c^0 \rightarrow \Xi^- \pi^+$	2.64 ± 0.13	-0.69 ± 0.03	4.08 ± 0.32	30.83 ± 0.84	-0.35 ± 0.11	1.80 ± 0.52 [21]	-0.64 ± 0.05
$\Xi_c^+ \rightarrow \Xi^0 \pi^+$	1.1 ± 0.3	-0.89 ± 0.15	2.49 ± 0.38	9.32 ± 1.24	0.47 ± 0.28	1.6 ± 0.8	
Channel	$10^2\mathcal{R}_X$	α	$ A $	$ B $	$\delta_P - \delta_S$	$10^2(\mathcal{R}_X)_{\text{exp}}$	α_{exp}
$\Xi_c^0 \rightarrow \Xi^- K^+$	4.08 ± 0.02	-0.73 ± 0.03	0.94 ± 0.07	7.10 ± 0.19	-0.35 ± 0.11	2.75 ± 0.57	
$\Xi_c^0 \rightarrow \Lambda K_S^0$	22.9 ± 1.4	-0.06 ± 0.37	1.96 ± 3.51	19.49 ± 2.93	-1.69 ± 0.68	22.9 ± 1.4 [22]	
$\Xi_c^0 \rightarrow \Sigma^0 K_S^0$	3.8 ± 0.7	0.12 ± 2.77	2.53 ± 1.16	4.45 ± 6.01	1.71 ± 8.84	3.8 ± 0.7 [22]	
$\Xi_c^0 \rightarrow \Sigma^+ K^-$	12.3 ± 1.2	-0.36 ± 3.96	0.69 ± 7.82	11.24 ± 4.51	-0.06 ± 2.54	12.3 ± 1.2 [22]	

that the fitting results for the branching fractions and decay asymmetries are in good agreement with experiment except for the following two modes: $\Xi_c^0 \rightarrow \Xi^- \pi^+$ and the ratio $\mathcal{R}_{\Xi^- K^+}$. Our predicted branching fraction of $(2.64 \pm 0.13)\%$ for $\Xi_c^0 \rightarrow \Xi^- \pi^+$ is noticeably higher than

the value of $(1.80 \pm 0.52)\%$ measured by Belle [21]. A similar result of $(2.72 \pm 0.09)\%$ has also been obtained in Ref. [8]. Indeed, the sum-rule relation derived in Eq. (8) is well satisfied by the fitting branching fractions listed in Table III.

As for the ratio $\mathcal{R}_{\Xi^- K^+}$, we see from Table I that in the SU(3) limit, one will have $\mathcal{R}_{\Xi^- K^+} = \sin^2 \theta_C$ which is equal to 0.045 after taking into account the phase-space difference between $\Xi_c^0 \rightarrow \Xi^- K^+$ and $\Xi_c^0 \rightarrow \Xi^- \pi^+$. The current measurement is 0.0275 ± 0.0057 which is away from the SU(3) expectation by 2σ . Since both modes proceed through the topological diagrams T and E_{1S} with the combination $2T - E_{1S} = 2\bar{T}$, it is conceivable that SU(3) breaking in the external W -emission T and especially in W -exchange E_{1S} will account for the discrepancy between theory and experiment.

If the pseudoscalar meson in the final-state is an SU(3) flavor-singlet η_1 , it will receive an additional contribution from the hairpin diagram E_h in Fig. 1. Numerically, we find that the combination $\tilde{E}_h = E_h + \frac{2}{3}E_{1S} - \frac{4}{3}E_{2S}$ which contributes only to η_1 is sizable (see Table II). Recall that in the charmed meson sector there is a strong indication

of the hairpin effect in the decay $D_s^+ \rightarrow \rho^+ \eta'$ (see e.g. Ref. [11]).

For the decay $\Lambda_c^+ \rightarrow \Xi^0 K^+$, we find $|A| = 4.46 \pm 0.29$, $|B| = 1.40 \pm 1.24$, both in units of $10^{-2}G_F$, and the phase difference $\delta_P - \delta_S = -2.10 \pm 0.91$ rad. Our predictions of $\mathcal{B}(\Lambda_c^+ \rightarrow \Xi^0 K^+) = (0.53 \pm 0.07)\%$ and $\alpha_{\Xi^0 K^+} = -0.07 \pm 0.14$ are consistent with the respective measurements of $(0.55 \pm 0.07)\%$ and 0.01 ± 0.16 [7]. Our results are to be compared with $\mathcal{B}(\Lambda_c^+ \rightarrow \Xi^0 K^+) = (0.40 \pm 0.03)\%$, $\alpha_{\Xi^0 K^+} = -0.15 \pm 0.14$ and $\delta_P - \delta_S = -2.06 \pm 0.50$ rad obtained in Ref. [8]. We have checked that if we set $\delta_S = \delta_P = 0$ from the outset and keep the measured $\alpha_{\Xi^0 K^+}$ as an input, the fit $\mathcal{B}(\Lambda_c^+ \rightarrow \Xi^0 K^+)$ of order 1×10^{-3} will be too small compared to experiment. On the contrary, if the input of $(\alpha_{\Xi^0 K^+})_{\text{exp}}$ is removed, the fit $\alpha_{\Xi^0 K^+}$ will be of order 0.95. Hence, we conclude that it is inevitable to introduce the phase shifts to accommodate the data.

4. Conclusion— We have performed a global fit to the experimental data of 2-body charmed baryon decays based on the topological diagrammatic approach and taken into account the phase shifts between S - and P -wave amplitudes. The measured branching frac-

tions and decay asymmetries are well accommodated in TDA except for two modes, in particular, the predicted $\mathcal{B}(\Xi_c^0 \rightarrow \Xi^- \pi^+) = (2.64 \pm 0.13)\%$ is larger than its current value. The fit results for the branching fraction, decay asymmetry and the phase shift $\delta_P - \delta_S$ for $\Lambda_c^+ \rightarrow \Xi^0 K^+$

TABLE IV. Same as Table III except for yet-to-be-measured modes.

Channel	$10^3\mathcal{B}$	α	$ A $	$ B $	$\delta_P - \delta_S$	Channel	$10^4\mathcal{B}$	α	$ A $	$ B $	$\delta_P - \delta_S$
$\Lambda_c^+ \rightarrow p K_L^-$	15.88 ± 0.69	0.34 ± 0.59	0.19 ± 0.08	0.30 ± 0.37	1.19 ± 0.74	$\Lambda_c^+ \rightarrow n K^+$	0.16 ± 0.04	-0.83 ± 0.18	0.13 ± 0.02	0.49 ± 0.07	0.47 ± 0.28
$\Xi_c^+ \rightarrow \Sigma^+ K_S^-$	5.65 ± 5.40	0.31 ± 0.54	3.55 ± 1.51	5.71 ± 6.99	1.19 ± 0.74	$\Xi_c^+ \rightarrow \Lambda^0 \pi^+$	5.02 ± 1.68	0.71 ± 0.18	0.46 ± 0.11	1.78 ± 0.34	-2.44 ± 3.16
$\Xi_c^+ \rightarrow p K_{S/L}^-$	4.86 ± 0.85	-0.46 ± 0.09	0.73 ± 0.14	5.97 ± 0.56	0.51 ± 4.28	$\Xi_c^+ \rightarrow n \pi^+$	0.42 ± 0.05	-0.14 ± 0.26	0.24 ± 0.02	0.07 ± 0.07	-2.10 ± 0.91
$\Xi_c^+ \rightarrow \Sigma^+ \pi^0$	2.18 ± 0.48	0.33 ± 0.34	0.62 ± 0.59	4.50 ± 0.74	-1.07 ± 0.58	$\Xi_c^+ \rightarrow \Sigma^0 K^+$	1.14 ± 0.06	-0.66 ± 0.03	0.15 ± 0.01	1.16 ± 0.03	-0.35 ± 0.11
$\Xi_c^+ \rightarrow \Sigma^+ \eta$	0.59 ± 0.72	0.17 ± 1.02	0.77 ± 0.37	1.65 ± 1.84	1.39 ± 1.11	$\Xi_c^+ \rightarrow p \pi^0$	0.22 ± 0.15	0.23 ± 0.42	0.03 ± 0.02	0.38 ± 0.13	-0.79 ± 4.34
$\Xi_c^+ \rightarrow \Sigma^+ \eta'$	4.02 ± 1.42	-0.33 ± 0.18	1.34 ± 0.46	10.97 ± 2.58	-1.99 ± 0.31	$\Xi_c^+ \rightarrow p \eta'$	2.46 ± 0.69	-0.35 ± 0.07	0.16 ± 0.03	1.23 ± 0.18	-2.29 ± 0.22
$\Xi_c^+ \rightarrow \Sigma^0 \pi^+$	3.03 ± 0.13	-0.6 ± 0.04	0.81 ± 0.07	5.22 ± 0.19	0.64 ± 0.08	$\Xi_c^+ \rightarrow p \eta'$	1.80 ± 0.50	-0.32 ± 0.38	0.20 ± 0.11	1.00 ± 0.23	1.14 ± 0.35
$\Xi_c^+ \rightarrow \Xi^0 K^+$	1.32 ± 0.19	-0.71 ± 0.11	1.27 ± 0.11	2.05 ± 0.32	-0.30 ± 0.19	$\Xi_c^+ \rightarrow \Lambda^0 K^+$	0.46 ± 0.06	-0.49 ± 0.10	0.19 ± 0.02	0.50 ± 0.04	-2.09 ± 0.11
$\Xi_c^0 \rightarrow \Sigma^0 K_L^-$	0.98 ± 0.19	0.21 ± 0.46	0.13 ± 0.12	0.96 ± 0.11	-1.26 ± 0.78	$\Xi_c^0 \rightarrow p K^-$	2.92 ± 1.01	-0.28 ± 3.14	0.16 ± 1.80	2.59 ± 1.04	-0.06 ± 2.54
$\Xi_c^0 \rightarrow \Xi^0 \pi^0$	14.3 ± 3.82	-0.10 ± 0.12	1.16 ± 0.40	24.27 ± 3.32	1.24 ± 0.80	$\Xi_c^0 \rightarrow n K_{S/L}^-$	6.04 ± 1.47	-0.33 ± 0.34	0.59 ± 1.52	5.16 ± 1.43	0.84 ± 2.16
$\Xi_c^0 \rightarrow \Xi^0 \eta$	2.78 ± 4.75	-0.19 ± 1.57	2.79 ± 4.22	8.04 ± 3.71	1.37 ± 1.57	$\Xi_c^0 \rightarrow \Lambda^0 \pi^0$	1.97 ± 2.10	-0.50 ± 0.62	0.59 ± 0.52	1.72 ± 0.49	-1.05 ± 0.74
$\Xi_c^0 \rightarrow \Xi^0 \eta'$	6.28 ± 4.46	0.42 ± 1.76	3.44 ± 2.75	14.97 ± 8.34	2.01 ± 3.88	$\Xi_c^0 \rightarrow n \pi^0$	0.04 ± 0.19	0.35 ± 0.83	0.11 ± 0.29	0.08 ± 0.27	-2.21 ± 3.81
$\Xi_c^0 \rightarrow \Lambda^0 K_L^-$	6.04 ± 0.47	-0.85 ± 1.08	0.11 ± 0.12	0.45 ± 0.24	0.45 ± 3.46	$\Xi_c^0 \rightarrow \Lambda^0 \eta$	4.59 ± 2.10	0.64 ± 0.47	0.53 ± 0.25	3.76 ± 0.99	-0.40 ± 1.30
$\Xi_c^0 \rightarrow \Sigma^+ \pi^-$	0.22 ± 0.03	-0.34 ± 3.75	0.16 ± 1.80	2.59 ± 1.04	-0.06 ± 2.54	$\Xi_c^0 \rightarrow \Lambda^0 \eta'$	3.28 ± 2.79	0.25 ± 1.83	0.98 ± 0.79	3.68 ± 1.57	1.82 ± 1.90
$\Xi_c^0 \rightarrow \Sigma^0 \pi^0$	0.34 ± 0.20	0.43 ± 0.58	0.26 ± 0.25	3.20 ± 0.86	-0.20 ± 3.72	$\Xi_c^0 \rightarrow \Sigma^- K^+$	0.77 ± 0.04	-0.65 ± 0.03	0.22 ± 0.02	1.64 ± 0.04	-0.35 ± 0.11
$\Xi_c^0 \rightarrow \Sigma^0 \eta$	0.16 ± 0.17	0.32 ± 1.35	0.64 ± 0.77	1.69 ± 0.87	-1.24 ± 1.39	$\Xi_c^0 \rightarrow p \pi^-$	0.18 ± 0.07	-0.27 ± 3.03	0.04 ± 0.41	0.60 ± 0.24	-0.06 ± 2.54
$\Xi_c^0 \rightarrow \Sigma^0 \eta'$	0.15 ± 0.07	0.36 ± 1.00	0.74 ± 0.41	2.76 ± 1.31	1.94 ± 3.41	$\Xi_c^0 \rightarrow n \eta$	0.20 ± 0.12	0.09 ± 1.29	0.21 ± 0.13	0.72 ± 0.23	1.67 ± 1.33
$\Xi_c^0 \rightarrow \Sigma^- \pi^+$	0.45 ± 0.02	-0.62 ± 0.03	0.47 ± 0.04	3.55 ± 0.10	-0.35 ± 0.11	$\Xi_c^0 \rightarrow n \eta'$	0.46 ± 0.20	-0.05 ± 0.43	0.01 ± 0.19	1.06 ± 0.24	0.59 ± 11.75
$\Xi_c^0 \rightarrow \Xi^0 K_{S/L}^-$	0.21 ± 0.09	-0.32 ± 1.93	0.52 ± 1.63	4.48 ± 1.71	-2.03 ± 1.89						

are consistent with the BESIII measurements. For yet-to-be-measured modes, we have presented the fitting magnitudes of S - and P -wave amplitudes and their phase shifts which can be tested in the near future.

ACKNOWLEDGMENTS

We would like to thank Pei-Rong Li and Chia-Wei Liu for valuable discussions. This research was supported in part by the Ministry of Science and Technology of R.O.C. under Grant No. MOST-112-2112-M-001-026 and the National Natural Science Foundation of China under Grant No. U1932104.

- [1] H. Y. Cheng, Chin. J. Phys. **78**, 324-362 (2022).
- [2] C. Q. Geng, C. W. Liu and T. H. Tsai, Phys. Lett. B **794**, 19-28 (2019).
- [3] H. Y. Cheng and B. Tseng, Phys. Rev. D **48**, 4188-4202 (1993).
- [4] H. Zhong, F. Xu, Q. Wen and Y. Gu, JHEP **02**, 235 (2023).
- [5] Z. P. Xing, X. G. He, F. Huang and C. Yang, Phys. Rev. D **108**, no.5, 053004 (2023).
- [6] J. Zou, F. Xu, G. Meng and H. Y. Cheng, Phys. Rev. D **101**, no.1, 014011 (2020).
- [7] M. Ablikim *et al.* [BESIII], Phys. Rev. Lett. **132**, 031801 (2024).
- [8] C. Q. Geng, X. G. He, X. N. Jin, C. W. Liu and C. Yang, [arXiv:2310.05491 [hep-ph]].
- [9] H. Y. Cheng and C. W. Chiang, Phys. Rev. D **81**, 074021 (2010); Phys. Rev. D **85**, 034036 (2012); Phys. Rev. D **86**, 014014 (2012); Phys. Rev. D **100**, 093002 (2019); Phys. Rev. D **104**, 073003 (2021).
- [10] H. Y. Cheng, C. W. Chiang and A. L. Kuo, Phys. Rev. D **93**, 114010 (2016).
- [11] H. Y. Cheng and C. W. Chiang, [arXiv:2401.06316 [hep-ph]].
- [12] X. G. He, Y. J. Shi and W. Wang, Eur. Phys. J. C **80**, no.5, 359 (2020).
- [13] Y. K. Hsiao, Y. L. Wang and H. J. Zhao, JHEP **09**, 035 (2022).
- [14] Y. Kohara, Phys. Rev. D **44**, 2799-2802 (1991).
- [15] L. L. Chau, H. Y. Cheng and B. Tseng, Phys. Rev. D **54**, 2132-2160 (1996).
- [16] Y. Kohara, [arXiv:hep-ph/9701287 [hep-ph]].
- [17] J. G. Korner, Nucl. Phys. B **25**, 282-290 (1971); J. C. Pati and C. H. Woo, Phys. Rev. D **3**, 2920-2922 (1971).
- [18] H.L. Zhong, F.R. Xu and H.Y. Cheng, in preparation.
- [19] R. L. Workman *et al.* [Particle Data Group], Prog. Theor. Exp. Phys. **2022**, 083C01 (2022) and 2023 update.
- [20] M. Ablikim *et al.* [BESIII], [arXiv:2311.06883 [hep-ex]].
- [21] Y. B. Li *et al.* [Belle], Phys. Rev. Lett. **122**, no.8, 082001 (2019).
- [22] Y. Li *et al.* [Belle], Phys. Rev. D **105**, no.1, L011102 (2022).
- [23] H. Dembinski and P. Ongmongkolkul *et al.* (2020), URL <https://doi.org/10.5281/zenodo.3949207>
- [24] F. James and M. Roos, Comput. Phys. Commun. **10**, 343 (1975).
- [25] S. X. Li *et al.* [Belle], Phys. Rev. D **107**, 032003 (2023).
- [26] L. K. Li *et al.* [Belle], Sci. Bull. **68**, 583-592 (2023).
- [27] M. Ablikim *et al.* [BESIII], JHEP **11**, 137 (2023).